Hindawi
International Journal of RF and Microwave Computer-Aided Engineering
Volume 2023, Article ID 8874001, 11 pages
https://doi.org/10.1155/2023/8874001

Research Article

A Low-Scattering Antenna Array at Both Normal and Grazing Incidence

Zhiyu Xing

School of Electronic Science and Engineering, University of Electronic Science and Technology of China, Chengdu 611731, China

Correspondence should be addressed to Zhiyu Xing; melonxzy_0715@163.com

Received 28 November 2022; Revised 9 January 2023; Accepted 13 April 2023; Published 21 April 2023

Academic Editor: Ali Gharsallah

In this paper, we investigate a low-scattering antenna array consisting of two different low radar cross-section (RCS) antenna elements. The low-scattering performance is achieved by broadband in-band absorbing with x (TM)-polarization and phase cancellation with y (TE)-polarization at normal incidence and a special shape design at grazing incidence. We demonstrate the effectiveness of the proposed antenna array through simulations and measurements. Compared with the reference one, the results show that it can achieve remarkable wideband monostatic RCS reduction from 3.3 to 8 GHz with a maximum reduction value of 23.5 dB at normal incidence and from 4.4 to 12.5 GHz with a peak reduction value of 15.3 dB at grazing incidence. Moreover, a low-RCS carrier is codesigned with the antenna array to verify the low-scattering property, which indicates that the proposed antenna array has a great potential for use in various application scenarios.

1. Introduction

As the electromagnetic windows of various stealth aircraft, antennas play important roles in modern warfare. The design of low radar cross-section (RCS) antenna while maintaining radiation performance has drawn great interest in recent years [1]. There are several methods for antenna RCS reduction (RCSR), mainly including loading varieties of artificial electromagnetic metamaterials and shape design.

For the former, the metasurfaces are usually positioned over or coplanar with the antennas, thus causing a relatively high profile or large dimension, respectively. For example, the widths of the coding metasurfaces composed by multiple types of artificial magnetic conductor (AMC) unit cells in [2, 3] are up to $4.7\lambda_0$ and $3.1\lambda_0$, respectively. Besides that, codesigned with high-performance partially reflecting surfaces (PRS), the profile heights of the integrated antennas in [4, 5] are $0.25\lambda_0$ and $0.44\lambda_0$ separately, whereas the traditional height of the microstrip antenna is less than $0.1\lambda_0$. Additionally, 64 metamaterial absorber (MA) unit cells are loaded surrounding a patch array in [6] to reduce the in-band RCS, leading to an inevitably increased aperture. The same situation appears in [7], where the MA-loading structure increases the lateral dimension of the antenna significantly. Similarly, the low-RCS antennas loaded with a planar phase gradient metasurface (PGM), an electromagnetic bandgap (EBG) structure, a polarization conversion surface (PCS), and a radome in [8–11], respectively, possess large horizontal sizes of $1.2\lambda_0$, $3.1\lambda_0$, $2\lambda_0$, and $1.6\lambda_0$ separately, whereas the common size of the antenna element is about $0.5\lambda_0$. In addition, when the periodic frequency selective surface (FSS) structure serves as the ground plane of the antenna, the profile or dimension of the integrated structure increases obviously. For instance, the dipole antenna loaded with a reconfigurable FSS reflector in [12] possesses a large size of $1.2\lambda_0$. The spiral antenna using a wideband FSS structure as the ground in [13] has an uncommon profile height of $0.25\lambda_0$. By comparison, there is no additional structure introduced in the method of

shape design. Considering that the integration of antenna with the carrier platform is essential in practical application, the shape method is more applicable to an antenna installation environment with limited size. For the shape design of single antennas, an octagonal-shaped UWB antenna with a performance of wideband RCS reduction is proposed in [14], which provides a referable research idea for the scholars. On this basis, an UWB antenna with an improved shape is designed in [15], and the bandwidth of the 10 dB RCS reduction is further broadened. In [16], a microstrip antenna with reduced in-band and out-of-band RCS is presented; partial areas of the patch and ground are subtracted to achieve the low-scattering performance. In sum up, although different shapes of single antennas in [14–16] can all achieve RCS reduction, the arrays are more widely in use in the stealth platforms owing to the properties of high gain and high directivity [17–20].

In [17], a rotation technique of antenna elements is utilized to achieve an in-band low-scattering property, but the RCS reduction is restricted to a narrow band, and this works only when the incident wave is circularly polarized. A 4×4 hybrid microstrip antenna array that employs two types of elements is proposed in [18]. The array possesses excellent radiation performance and meanwhile achieves remarkable monostatic RCS reduction in a wide frequency band from 4 to 8 GHz for normal incidence. The only pity is that the scattering property at grazing incidence of electromagnetic waves is not carefully studied and discussed. In fact, the case of grazing incidence is common and worth researching in the radar detection field which happens when the horizontal detection distance is far greater than the vertical height difference. Zhao et al. [19] proposed a 4×4 antenna array and favorable results are obtained in addressing the conflict between radiation and scattering; however, the size of the MS-based element is up to $0.67\lambda_0$ which is relatively large and harmful to the wide-angle scanning of antenna array. The same thing exists in [20], where an integrated 4×4 dipole array with electromagnetic wave absorbing function is proposed to realize wide out-of-band RCSR property, but the element spacing is more than $0.6\lambda_0$.

To solve the problems mentioned above, we propose a low-scattering 4×4 hybrid antenna array operating at both normal and grazing incidence. There are no extra structures being introduced in the design process; only the shapes of the microstrip antenna elements are changed (compared with the reference ones). Finally, experiment results demonstrate that the proposed hybrid array with a simple structure possesses a small element spacing, maintains good radiation performance, and meanwhile achieves broadband in- and out-of-band RCS reduction at both normal and grazing incidence.

This paper is organized as follows: the design and performance of the two antenna elements are given in Section 2. In Section 3, the reference and low-scattering antenna arrays are introduced, besides that, electrical and scattering performances comparison between them both is provided. A comparison of the proposed hybrid array with the published low-RCS arrays is presented in Section 4. Section 5 is the conclusion.

2. Design and Performance of the Two Antenna Elements

2.1. Structure and Working Principle. The structures of the two proposed low-RCS antenna elements are shown in Figures 1(a) and 1(b), respectively, and a reference antenna is designed for comparison, as presented in Figures 1(c) and 1(d). A simple coaxial back-fed method and an F4BM substrate (relative permittivity 2.2 and thickness 6 mm) are adopted for three antennas. In addition, Figure 1(e) depicts the schematic diagram of the incoming electromagnetic waves at normal and grazing incidence (with two polarizations separately) in detail. It is noted that the reference antenna must be designed for comparison to reflect the good low-scattering performance of the two proposed antenna elements. Considering that the two elements are microstrip antennas, the reference antenna is specified as a square patch microstrip antenna with the same size and feeding method as the proposed elements for a fair comparison. In [17, 18], the reference antennas are also selected as square patch microstrip antennas, which proves the rationality of our reference antenna design in this paper.

Under normal incidence with x-polarization, the low-scattering performance of antennas A and B is obtained by the inherent in-band matching absorption principle. Here, both antennas are connected to 50 Ω-matched loads, because the antenna elements are x-polarized, the incident waves are partially absorbed by the antenna elements. Accordingly, the feeding points are arranged on the x-axis to produce x-polarized wave radiation. When the incident waves are y-polarized, the two antennas have almost the same reflection magnitudes and an approximately 180° reflection phase difference in a wide frequency range, which means that a broadband RCS reduction can be achieved by the phase cancellation principle when the two antenna subarrays are placed alternately one after another to form a chessboard configuration. The phase cancellation principle is introduced with detail in [2]. Hence, the distances between two nonradiative edges (along the y-direction) for antennas A and B are specially designed. For the former, the nonradiative edges are narrowed to increase the 0° reflection phase frequency. For the latter, a U-shaped slot etched on the radiation patch and a strip slot cut on the ground plane are introduced to bring down the resonance frequency and change the trend of the reflection phase curve, making the sole 0° phase reflection frequency of antenna A close to the reflection phase inverse frequency of antenna B and meanwhile broadening the region of $180° \pm 37°$ reflection phase difference.

When the aircraft performs penetration operations, the horizontal distance between the platform and the radar is usually far greater than the height difference between them, which makes the radar waves irradiate the antenna (installed on the platform) at a large angle of incidence called the grazing incidence. In this case, the threat area of the monostatic radar is usually limited to a range of ±25° in azimuth and ±15° in pitch in the forward angle domain of the platform. As the representative angles, the 0° azimuth angle and 5°pitch angle refer to $\varphi = 270°$ and $\theta = 85°$ separately, in Figure 1(e), and the RCS reduction of grazing incidence with

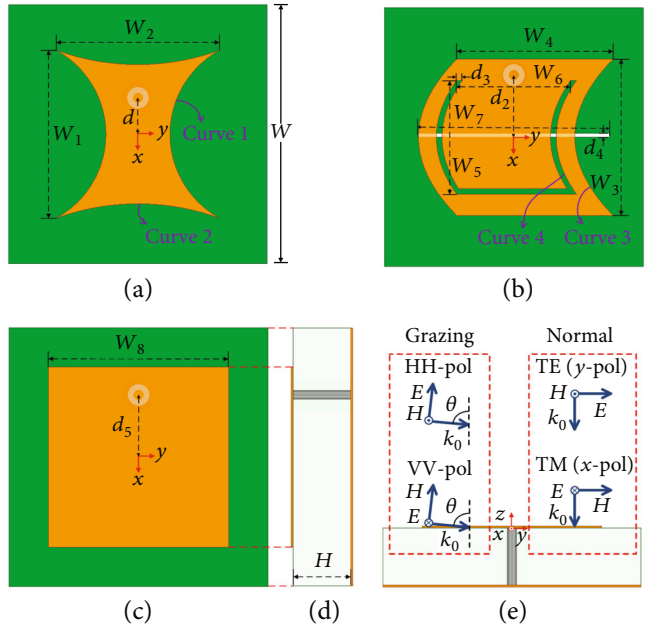

Figure 1: Geometry of the proposed antenna elements. (a) Antenna A. (b) Antenna B. (c) Reference antenna. (d) Side view of the reference antenna. (e) Polarization modes of the incoming waves at normal and grazing incidence.

Table 1: Parameters for the proposed antenna elements. (unit: mm).

Symbol	Value	Symbol	Value	Symbol	Value
W	27	W_6	11.9	d_4	0.115
W_1	17.5	W_7	20	d_5	6.5
W_2	17	W_8	18.8	H	6
W_3	16.3	d	3.8	r	10
W_4	16.3	d_2	6.5	t	25
W_5	11.9	d_3	0.6	a = b	60 (/)

the specific incident angle is studied in this paper. To effectively reduce the monostatic RCS for both antennas under large-angle grazing incidence, the circular arc-shaped and parabolic-shaped non-radiation edges of the patches are well designed and optimized to form antennas A and B, respectively. Compared with conventional straight edges, they can reflect the incoming electromagnetic waves to other nonthreatening angle domain effectively with a relatively wide frequency bandwidth. The physical idea of the shape design at grazing incidence could be reflected in many other applications. For example, the array antenna of airborne fire control radar is usually inclined, and the monostatic RCS of frequency-selective surface radome is usually reduced through the similar shape design. The functions of the shape curves 1 to 4 presented in Figures 1(a) and 1(b) can be expressed as

$$y = \sqrt{r^2 - \left(\frac{w_1}{2}\right)^2} - \sqrt{r^2 - x^2} + \frac{w_2}{2}, x \in \left[-\frac{w_1}{2}, \frac{w_1}{2}\right], \quad (1)$$

$$x = \sqrt{t^2 - \left(\frac{w_2}{2}\right)^2} - \sqrt{t^2 - y^2} + \frac{w_1}{2}, x \in \left[-\frac{w_2}{2}, \frac{w_2}{2}\right], \quad (2)$$

$$y = a \bullet x^2 - a \bullet \left(\frac{w_3}{2}\right)^2 + w_4/2 + 2.2, x \in \left[-\frac{w_3}{2}, \frac{w_3}{2}\right], \quad (3)$$

$$y = b \bullet x^2 - b \bullet \left(\frac{w_5}{2}\right)^2 + w_6/2 + 2.2, x \in \left[-\frac{w_5}{2}, \frac{w_5}{2}\right], \quad (4)$$

where r and t represent the arc radiuses, and a and b are coefficients of the two parabolic equations separately. The four parameters above are optimized to achieve low-RCS performance at grazing incidence. Other structure parameters shown in Figure 1 are provided in Table 1.

2.2. Performance of the Antenna Elements. All the numerical simulations were implemented with commercial high-frequency structure simulator software. To make the hybrid antenna array composed of antennas A and B have both good electrical and scattering properties, the resonance frequencies of the two antennas should be the same. Figure 2 shows the simulated reflection coefficient and radiation patterns, demonstrating that antennas A and B are resonant at the same frequency of 4.8 GHz and that the radiation patterns in the xoz-plane and yoz-plane are similar.

The simulated reflection performances of the two antennas with matched loads at normal incidence are given in

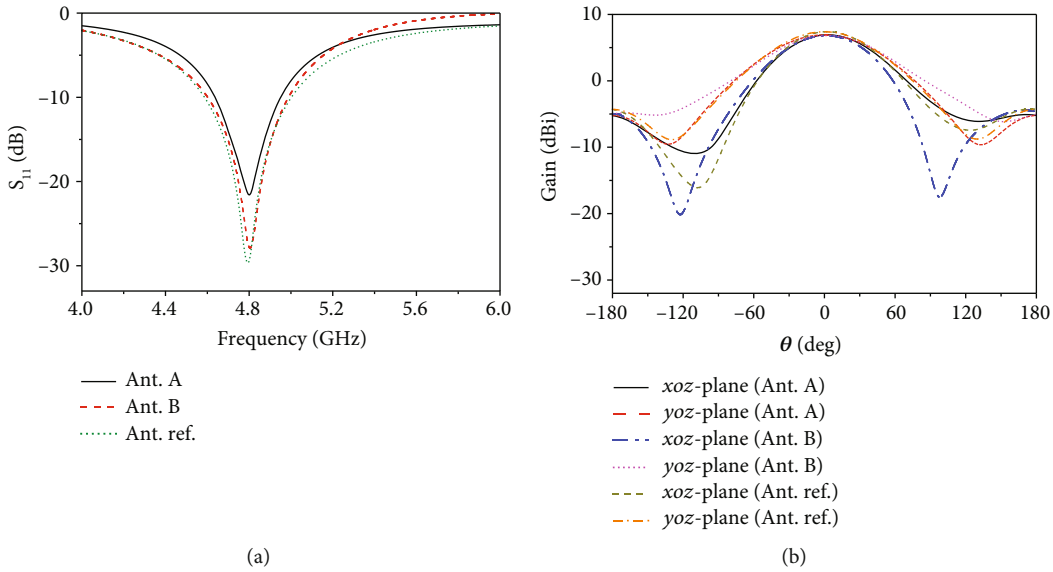

FIGURE 2: Simulated electrical performances of the two antennas. (a) Reflection coefficient. (b) 2-D radiation patterns at 4.8 GHz.

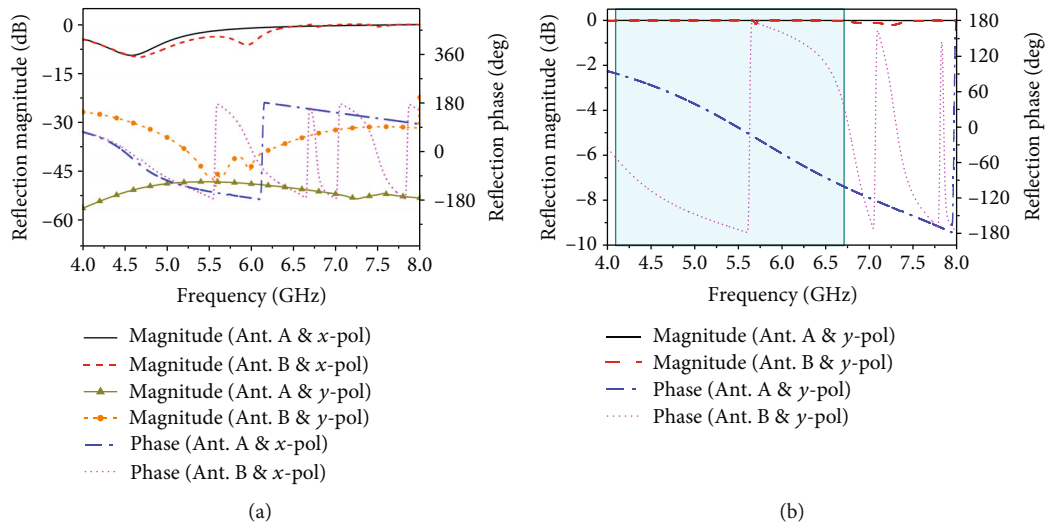

FIGURE 3: Simulated reflection performances of the two antennas at normal incidence with (a) x-polarization. (b) y-polarization.

Figure 3. For the x-polarization, we can see from Figure 3(a) that the co-polarization (x-polarization) reflection magnitude curves of the two antennas have troughs around 4.7 GHz owing to the in-band absorption characteristic. Considering that the proposed antenna B is asymmetric and polarization conversion could likely occur when the incident waves illuminate with the x-polarization, we also give the reflection magnitudes of the cross-polarized waves (y-polarization) in Figure 3(a) to quantify if a substantial part of the incident wave power is reflected in the orthogonal polarization. We observe that the reflection magnitudes of the cross-polarized waves are extremely small, which verifies that there is almost no polarization conversion occurring and the incident wave power is mainly absorbed. For the y-polarization, the two antennas possess an almost total copolarization (y-polarization) reflection property from 4 to 8 GHz, as shown in Figure 3(b). Furthermore, the antenna A has the sole 0° reflection phase at 5.5 GHz which is close to the reflection phase inverse frequency of 5.6 GHz of the antenna B. The area of effective phase difference staying in the range of 180° ± 37° is filled with blue, so we infer that the potential bandwidth for a 10-dB RCS reduction of the hybrid array ranges from 4.1 to 6.7 GHz.

The physical reason for the proposed shape of the array elements at normal incidence could be explained by the simulated surface current distribution shown in Figure 4. We see from Figures 4(a) and 4(b) that the induced currents mainly flow along the x-direction with x-polarized illumination, thus the incident waves are partially absorbed by the antenna elements. In Figures 4(c) and 4(d), the current path on the patch with the U-shaped slot is longer than that of the patch without the U-shaped slot, leading to a lower resonant frequency.

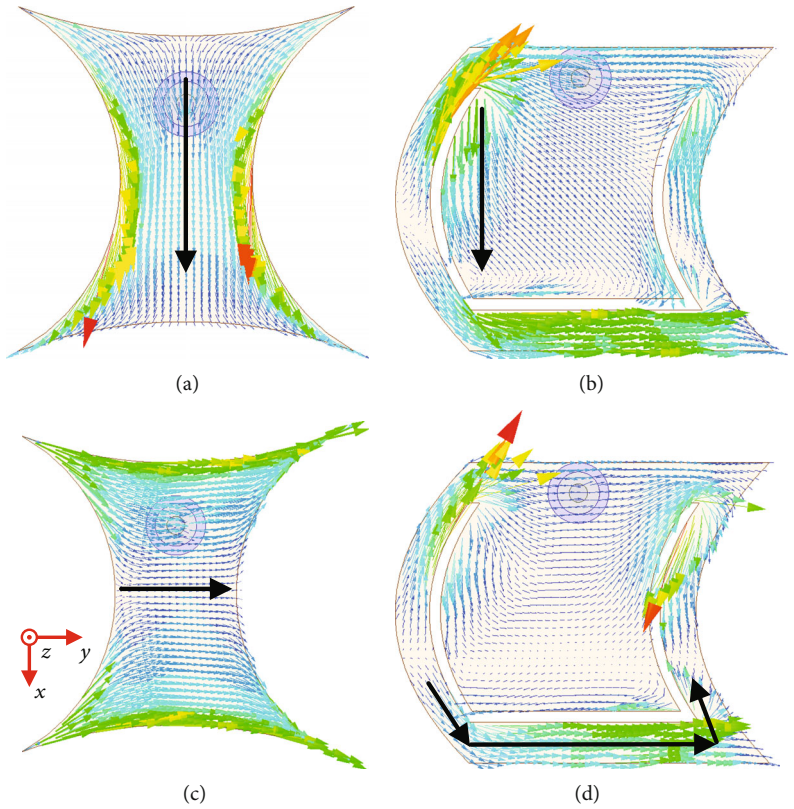

FIGURE 4: Simulated surface current distribution for two antennas at normal incidence. (a) Antenna A with x-polarization at 4.7 GHz. (b) Antenna B with x-polarization at 4.7 GHz. (c) Antenna A with y-polarization at 5.5 GHz. (d) Antenna A with y-polarization at 5.5 GHz.

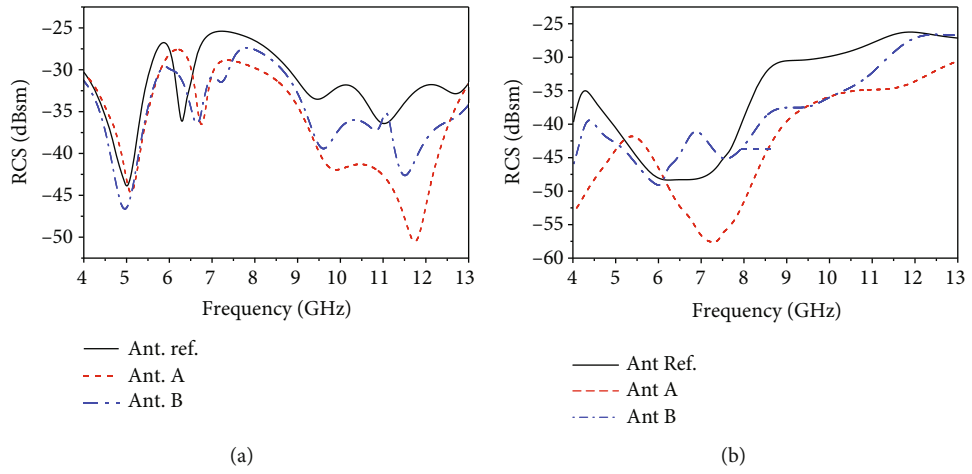

FIGURE 5: Simulated monostatic RCS versus frequency at grazing incidence ($\theta = 85^\circ$, $\varphi = 270^\circ$). (a) VV-polarization. (b) HH-polarization.

Consequently, the frequency point where the reflection phase is zero shifts to the lower frequency band, and then an effective phase difference in a wide frequency band is produced.

The simulated monostatic RCS versus frequency at grazing incidence ($\theta = 85^\circ$, $\varphi = 270^\circ$) are plotted in Figure 5. For the VV-polarization, the monostatic RCS of the two proposed antennas is much lower than that of the reference antenna in a wide frequency range from 6.6 to 12.8 GHz with a peak RCSR value of 18.2 dB at 11.8 GHz. For the HH-polarization, a remarkable RCS reduction is achieved from 7.7 to 12.2 GHz. The simulated results demonstrate that the introduction of special shape in antennas A and B brings the dramatic scattering performance improvements at grazing incidence.

3. Design and Performance Comparison of the Reference Array and Low-Scattering Array

3.1. Structure and Electrical Performance Comparison. As presented in Figure 6(b), the low-scattering hybrid array

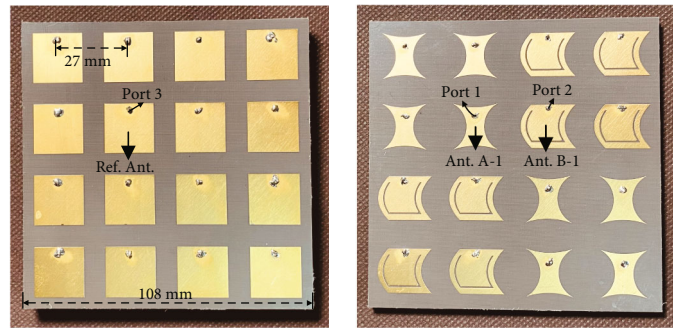

FIGURE 6: Photographs of the proposed reference and low-scattering arrays. (a) Photograph of reference array. (b) Photograph of hybrid array.

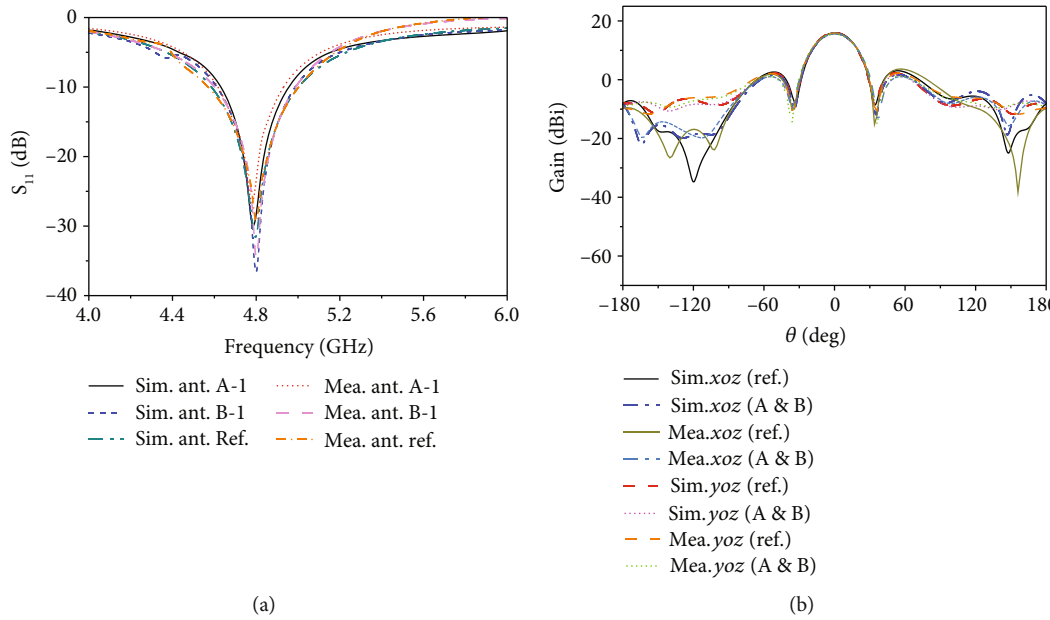

FIGURE 7: Simulated and measured electrical performance of both arrays. (a) Reflection coefficient. (b) Radiation patterns of both arrays at 4.8 GHz.

contains 2×2 subarrays with overall dimensions of 108 mm $\times$ 108 mm. To achieve wideband RCS reduction by the principle of destructive interference, two types of subarrays are placed alternately, one after another, to form a chessboard configuration. The reference array composed of 4×4 reference antenna elements is fabricated for comparison, as given in Figure 6(a).

Figure 7 shows the electrical performance of the reference and hybrid antenna arrays. The antennas A-1 and B-1 in the hybrid array shown in Figure 6(b) are selected and excited via port 1 and port 2 separately to observe the reflection coefficient (S_{11}). A reference antenna is selected and fed via port 3 for comparison, as shown in Figure 6(a). We see from Figure 7(a) that the simulated S_{11} curves are almost consistent with the measured ones, and they are all resonant at the central frequency of 4.8 GHz. The radiation patterns of both arrays at 4.8 GHz are given in Figure 7(b). It is observed that the simulated radiation patterns of the hybrid array are in good agreement with those of the reference array. The peak gains of the hybrid and reference arrays are 16.0 dBi and 15.9 dBi, respectively, indicating that only a 0.1 dB gain loss is caused. We conclude that the hybrid array composed of antennas A and B maintains good radiation performance in comparison with the reference array. In addition, although the measured radiation patterns have some small differences in trends from the simulated ones, the 3 dB beamwidths and maximum gains are nearly the same in both cases.

3.2. Scattering Performance Comparison. Figure 8 shows the simulated and measured scattering performances of both arrays at normal incidence of plane waves. We observe from Figure 8(a) that the proposed hybrid array achieves both in-band and out-of-band monostatic RCS reduction with *x*-polarization in a wide frequency band from 3.3 to 8 GHz. The simulated maximum value of RCS reduction is 10.5 dB

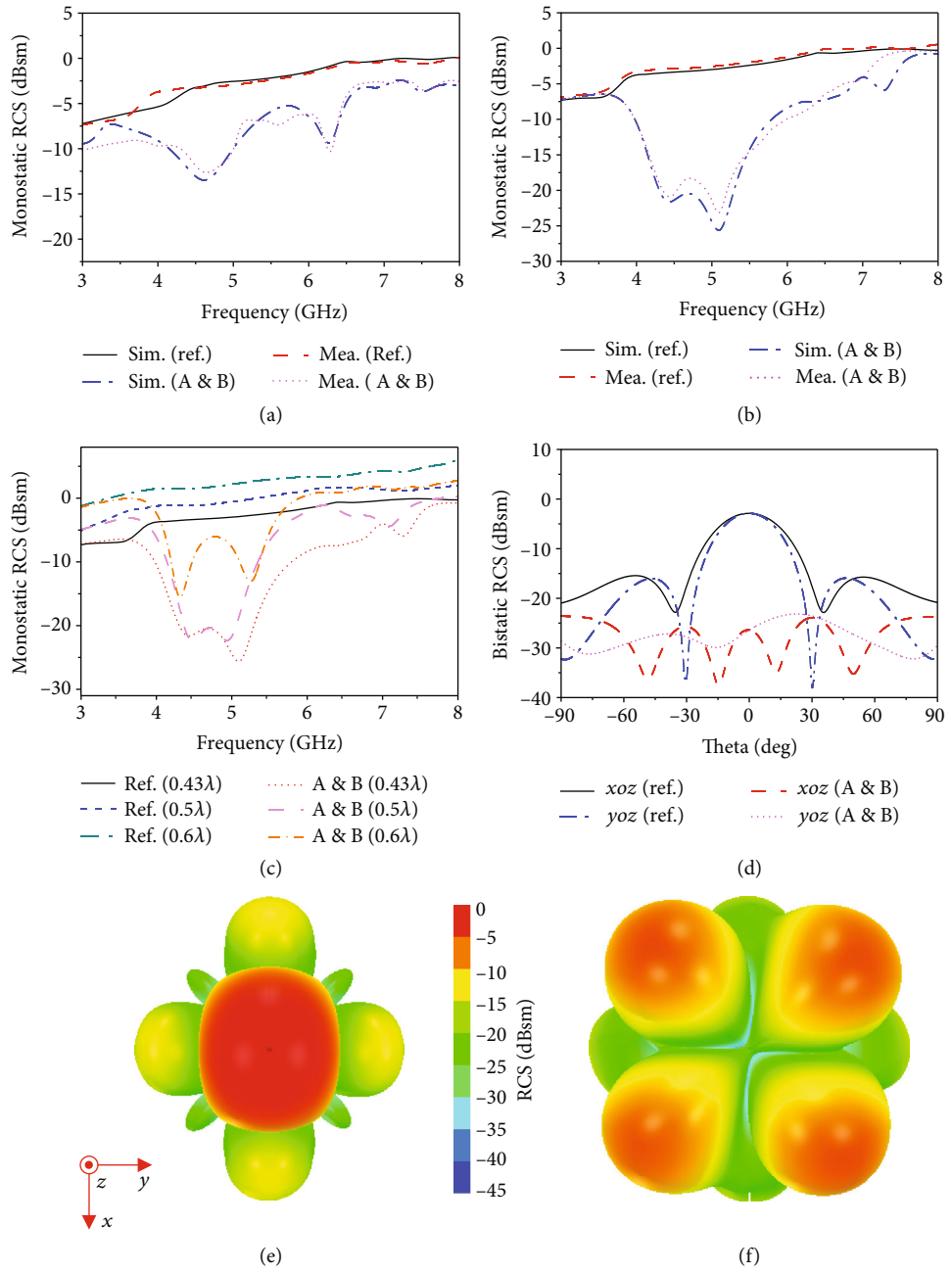

Figure 8: Simulated and measured scattering performance of both arrays at normal incidence. (a) Monostatic RCS with x-polarization. (b) Monostatic RCS with y-polarization. (c) Monostatic RCS with y-polarization under different element spacing. (d) 2-D bistatic RCS patterns with y-polarization at 5.1 GHz. (e) 3-D bistatic RCS patterns of the reference array with y-polarization at 5.1 GHz. (f) 3-D bistatic RCS patterns of the hybrid array with y-polarization at 5.1 GHz.

at 4.7 GHz, whereas the average reduction value is 5.2 dB. For the y-polarization, the monostatic RCS of the hybrid array is much lower than that of the reference array from 3.7 to 8 GHz due to the wideband reflection phase cancellation introduced by the antennas A and B. Furthermore, the bandwidth range of 10-dB RCS reduction is from 4.1 to 5.7 GHz with a peak RCSR value of 23.5 dB at 5.1 GHz. Figure 8(c) presents the change in scattering response (with y-polarization) due to the change of array element spacing. With the increase of the element spacing from $0.43\lambda_0$ to $0.6\lambda_0$, the monostatic RCS for the reference and hybrid arrays is increased, whereas the value of RCS reduction by the principle of destructive interference is decreased. This is because as the spacing increases, the effective reflection phase difference between antennas A and B changes, and the performance of passive phase cancellation in a wide frequency band is degraded. Consequently, the hybrid array with an element spacing of $0.43\lambda_0$ (equal to the width of the proposed elements A and B) is the most reasonable. During the measurement, two pairs of horn antennas (3.9-5.8 GHz and 5.8-8.5 GHz) are utilized to

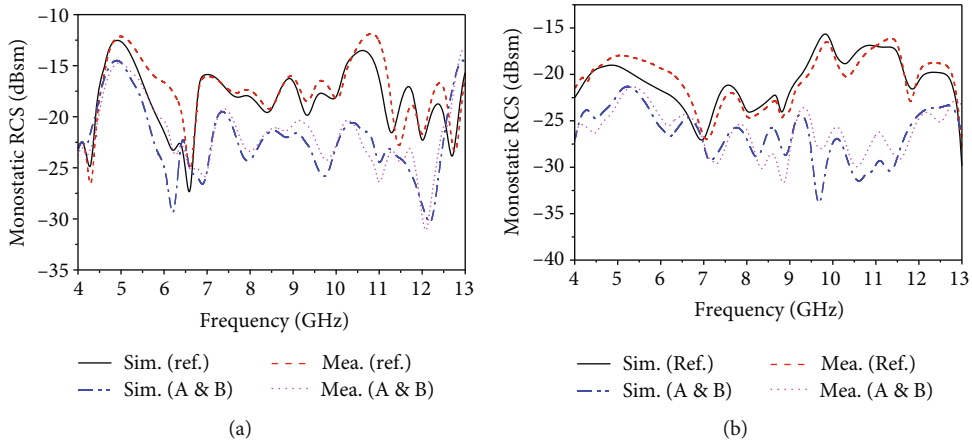

FIGURE 9: Simulated and measured monostatic RCS of both arrays at grazing incidence. (a) VV-polarization. (b) HH-polarization.

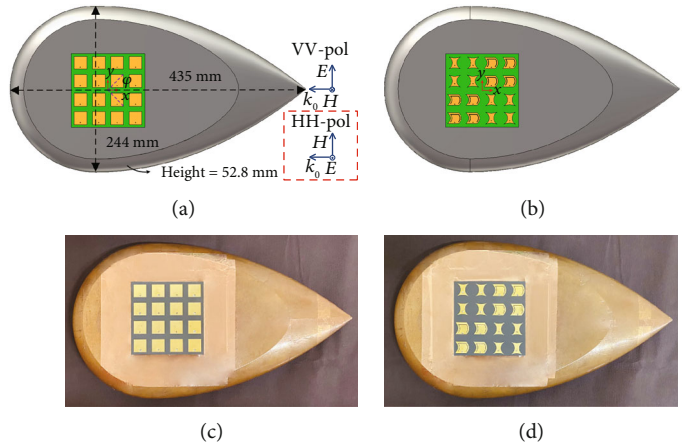

FIGURE 10: Simulation models and photographs of the two types of integrated structures. (a) Model of the reference array. (b) Model of the hybrid array. (c) Photograph of the reference array. (d) Photograph of the hybrid array.

transmit and receive the electromagnetic wave in the anechoic chamber, and meanwhile, both the antenna arrays are loaded with the matched loads. It is worth mentioning that the measured monostatic RCS results are in good agreement with the simulated ones.

The 2-D bistatic RCS patterns with y-polarization at 5.1 GHz are presented in Figure 8(d). We can observe that the maximum bistatic RCS of the hybrid array in the xoz-plane is 20.7 dB less than that of the reference array, whereas the value is 20.3 dB in the yoz-plane. The 3-D bistatic RCS patterns with y-polarization are given in Figures 8(e) and 7(f). We see that the bistatic RCS of the hybrid array is dramatically reduced along the principal planes, and meanwhile, four main scattering lobes appear at the four quadrants instead of the single main lobe, which also reflects the performance of destructive interference achieved by the hybrid array.

Figure 9 gives the simulated and measured monostatic RCS of both arrays at grazing incidence ($\theta = 85°$, $\varphi = 270°$). Compared with the reference array, remarkable RCS reduction is achieved from 4.4 to 12.5 GHz with both VV- and HH-polarizations for the hybrid array. The RCSR peaks are 11.7 dB at 12.2 GHz and 15.3 dB at 10.6 GHz, respectively, whereas the average RCS reduction values are 5.1 dB and 6.2 dB separately.

3.3. Low-RCS Carrier Codesigned with the Low-Scattering Antenna Array at Grazing Incidence. To verify the low-scattering performance of the proposed hybrid array at grazing incidence in the actual combat scenarios, a low-RCS amygdala carrier is codesigned with the array to form an integrated aircraft local platform. The dimensions of the platform are 435 mm in length, 244 mm in width, and 52.8 mm in height. The upper surface of the integrated platform is flat with an antenna array installed in a square cavity. Illuminated by the plane wave at grazing incidence, the two types of integrated structures show different scattering performances. The simulated models and photographs of the integrated structures are illustrated in Figure 10. Figure 11 shows the monostatic RCS of the integrated structures versus θ and φ with both VV- and HH-polarizations. Note that the azimuth angle φ varying from 0° to 25° and θ varying from 75° to 90° are investigated in the xoy- and xoz-planes separately.

In the xoz-plane with VV-polarization, we see from Figure 11(a) that the simulated RCS of the proposed

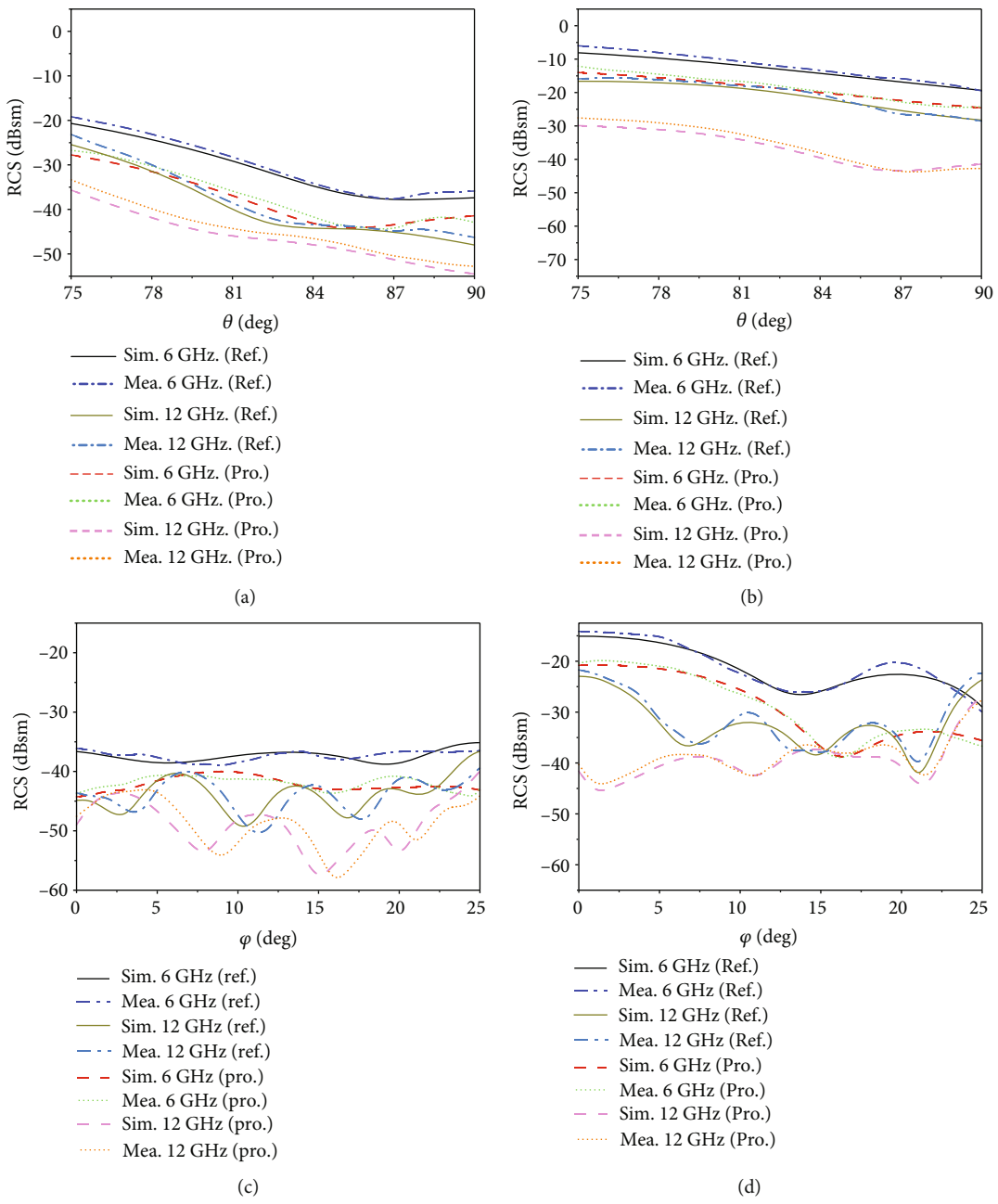

Figure 11: Simulated and measured monostatic RCS of the integrated structures. (a) Versus θ with VV-polarization. (b) Versus θ with HH-polarization. (c) Versus φ with VV-polarization. (d) Versus φ with HH-polarization.

integrated structure is lower than that of the reference one in the whole θ angle domain, and the average RCSR values reach 6.8 dB at 6 GHz and 6.2 dB at 12 GHz, respectively. Besides that, the varying trend of the RCS curves with HH-polarization is similar; as the incident angle θ increases, the monostatic RCS is reduced gradually. However, the average RCSR at 12 GHz reaches 15.6 dB. In the xoy-plane, remarkable RCS reduction is achieved in the whole φ angle domain for both polarizations. The simulated peak RCSR values are 7.6 dB at 6 GHz and 14.9 dB at 12 GHz separately with VV-polarization, whereas the maximum RCSR values are 14.7 dB at 6 GHz and 22.9 dB at 12 GHz with HH-polarization. Although there are some slight differences between the simulated and measured results, the varying trends of the monostatic RCS are almost the same in both cases. Therefore, the low-scattering performance of the integrated structure composed of a hybrid array and a low-RCS carrier is fully demonstrated.

4. Comparison of the Proposed Array with the Published Low-RCS Arrays

Table 2 shows a comparison of the previously reported low-RCS arrays and our proposed hybrid array in terms of incidence way, antenna element spacing, RCSR bandwidth, in-band RCSR value, and with or without extrastructure.

Table 2: Comparison of the proposed array with the published low-RCS arrays.

Ref.	Incidence way	Element spacing	RCSR band (GHz)	In-band RCSR (dB)	Extrastructure
[17]	Normal	$0.57\lambda_0$	10	10	No
[18]	Normal	$0.5\lambda_0$	4-8	13	No
[19]	Normal	$0.67\lambda_0$	4-8	9.5	No
[20]	Normal	$0.6\lambda_0$	3-5; 6-10	0	No
[10]	Normal	$0.5\lambda_0$	9-40	0	Yes
[11]	Normal	$0.65\lambda_0$	4.5-13.5	8.5	Yes
Our work	**Normal & Grazing**	**$0.43\lambda_0$**	**3.3-8 &4.4-12.5**	**17.8**	**No**

As a note, in this paper and in [17–20], the low-scattering performances of the arrays are achieved by the method of shape design, thus there are no extrastructures being introduced and the arrays have a simple and compact structure. Compared with the arrays in [17–19], our proposed array simultaneously realizes RCS reduction at both normal and grazing incidence, has a broader RCSR frequency range, and possesses a better in-band RCSR characteristic. Besides that, the array has a minimum element spacing as small as $0.43\lambda_0$ while maintaining good radiation performance. To better reflect its advantages, we list the refs. [10, 11] as comparative examples here. The arrays in [10, 11] are loaded with different artificial electromagnetic metasurfaces which are extrastructures and result in an increase of array aperture. Besides that, the arrays usually cannot realize the in-band RCS reduction, although they possess broader out-of-band RCSR frequency bands. By comparison, our proposed array has a simpler structure and smaller element spacing. In addition, it can achieve remarkable in-band and out-of-band RCS reduction at both normal and grazing incidence. From the above comparison and contrast, we see that the proposed low-scattering 4×4 hybrid antenna array can operate at both normal and grazing incidences, and meanwhile, it realizes the integration design of good radiation and scattering performance without introducing additional metasurfaces or increasing the element spacing.

5. Conclusions

A low-scattering antenna array consisting of two types of low-RCS antenna elements is investigated in this paper. The proposed hybrid array with a simple structure and small element spacing possesses broadband absorbing characteristics and can achieve destructive interference with x- and y-polarization separately at normal incidence, whereas the monostatic RCS at grazing incidence is sharply reduced by a special shape design. The results show that the hybrid array maintains good radiation performance with only a 0.1 dB gain deterioration at the central frequency. Also, remarkable in- and out-of-band RCS reductions are achieved from 3.3 to 8 GHz at normal incidence and from 4.4 to 12.5 GHz at grazing incidence, respectively. Furthermore, a low-RCS carrier is codesigned with the proposed array, which makes us believe that it can be used in various actual combat scenarios.

Data Availability

Data sharing is not applicable to this article as no new data were created or analyzed in this study.

Conflicts of Interest

The authors declare that they have no conflicts of interest.

Acknowledgments

This work was supported in part by the Joint Fund of Equipment Pre-Research of Aerospace Science and Technology under Grant 6141B061008.

References

[1] E. F. Knott, J. F. Shaeffer, and M. T. Tuley, *Radar Cross Section*, Scitech Publications, Raleigh, NC, USA, 2004.

[2] M. Abdullah and S. Koziel, "Supervised-learning-based development of multibit RCS-reduced coding metasurfaces," *IEEE Transactions on Microwave Theory and Techniques*, vol. 70, no. 1, pp. 264–274, 2022.

[3] M. Mighani and G. Dadashzadeh, "Broadband RCS reduction using a novel double layer chessboard AMC surface," *Electronics Letters*, vol. 52, no. 14, pp. 1253–1255, 2016.

[4] L. Zhang and T. Dong, "Low RCS and high-gain CP microstrip antenna using SA-MS," *Electronics Letters*, vol. 53, no. 6, pp. 375-376, 2017.

[5] H. Jiang, Z. Xue, M. Leng, W. Li, and W. Ren, "Wideband partially reflecting surface antenna with broadband RCS reduction," *IET Microwaves, Antennas & Propagation*, vol. 12, no. 6, pp. 941–946, 2018.

[6] Z. Xing, F. Yang, P. Yang, and J. Yang, "A low-RCS and wideband circularly polarized array antenna co-designed with a high-performance AMC-FSS radome," *IEEE Antennas and Wireless Propagation Letters*, vol. 21, no. 8, pp. 1659–1663, 2022.

[7] Y. Zhou, X. Cao, J. Gao, Y. J. Zheng, H. H. Yang, and S. J. Li, "Broadband aperture-coupling patch antenna with improved radiation and scattering performance based on metamaterial absorber," *IET Microwaves, Antennas & Propagation*, vol. 13, no. 7, pp. 875–880, 2019.

[8] B. Li, X. Liu, H. Shi, C. Yang, Q. Chen, and A. Zhang, "Planar phase gradient metasurface antenna with low RCS," *IEEE Access*, vol. 6, pp. 78839–78845, 2018.

[9] Z. Han, W. Song, and X. Sheng, "Gain enhancement and RCS reduction for patch antenna by using polarization-dependent

EBG surface," *IEEE Antennas and Wireless Propagation Letters*, vol. 16, pp. 1631–1634, 2017.

[10] E. Ameri, S. H. Esmaeli, and S. H. Sedighy, "Ultra wideband radar cross section reduction by using polarization conversion metasurfaces," *Scientific Reports*, vol. 9, no. 1, p. 478, 2019.

[11] S. Sun, W. Jiang, X. Li, P. Liu, and S. Gong, "Ultrawideband high-efficiency 2.5-dimensional polarization conversion metasurface and its application in RCS reduction of antenna," *IEEE Antennas and Wireless Propagation Letters*, vol. 18, no. 5, pp. 881–885, 2019.

[12] F. Wang, K. Li, Y. Ren, and Y. Zhang, "A novel reconfigurable FSS applied to the antenna radar cross section reduction," *International Journal of RF and Microwave Computer-Aided Engineering*, vol. 29, no. 7, article e21729, 2019.

[13] T. Hong, W. Jiang, S. Gong, X. Wang, and S. Zhang, "Single-layer wideband FSS for the RCS reduction of spiral antenna," *Journal of Electromagnetic Waves and Applications*, vol. 29, no. 16, pp. 2191–2198, 2015.

[14] C. M. Dikmen, S. Çimen, and G. Çakir, "Planar octagonal-shaped UWB antenna with reduced radar cross section," *IEEE Transactions on Antennas and Propagation*, vol. 62, no. 6, pp. 2946–2953, 2014.

[15] M. Khorramizadeh and S. M. A. Nezhad, "Low-RCS feature for UWB antenna with bandnotch characteristics," *Journal of Electromagnetic Waves and Applications*, vol. 35, no. 2, pp. 198–207, 2021.

[16] J. Zhang, J. Xu, Y. Qu, J. Ding, and C. Guo, "A microstrip antenna with reduced in-band and out-of-band radar cross-section," *International Journal of Microwave and Wireless Technologies*, vol. 11, no. 2, pp. 199–205, 2019.

[17] P. Yang, F. Yan, F. Yang, and T. Dong, "Microstrip phased-array in-band RCS reduction with a random element rotation technique," *IEEE Transactions on Antennas and Propagation*, vol. 64, no. 6, pp. 2513–2518, 2016.

[18] Y. Liu, Y. Jia, W. Zhang, Y. Wang, S. Gong, and G. Liao, "An integrated radiation and scattering performance design method of low-RCS patch antenna array with different antenna elements," *IEEE Transactions on Antennas and Propagation*, vol. 67, no. 9, pp. 6199–6204, 2019.

[19] Y. Zhao, X. Cao, J. Gao, L. Xu, X. Liu, and L. Cong, "Broadband low-RCS circularly polarized array using metasurface-based element," *IEEE Antennas and Wireless Propagation Letters*, vol. 16, pp. 1836–1839, 2017.

[20] C. Jin, B. Zhang, L. Yin, Q. Lv, L. Kong, and L. Li, "Integrated low-profile low radar cross section circularly polarized dipole antenna array," *IEEE Transactions on Antennas and Propagation*, vol. 69, no. 12, pp. 8461–8469, 2021.